COMMUNICATION

CrossMark
click for updates

Highly nanoporous silicas with pore apertures near the boundary between micro- and mesopores through an orthogonal self-assembly approach†

Koki Muraoka,[a] Watcharop Chaikittisilp,*[a] Yutaka Yanaba,[b] Takeshi Yoshikawa[b] and Tatsuya Okubo*[a]

Nanoporous silicas having some periodicity, high surface area (up to 1230 m² g⁻¹), and pore diameters near the boundary between micro- and mesopores are synthesized using aromatic compounds bearing anionic end-groups as novel structure-directing agents (SDAs) that can facilitate multiple interactions between SDAs, co-SDAs and silica frameworks orthogonally.

Silica-based nanoporous materials, including zeolite and mesoporous silica, are one of the most important class of nanoporous materials mainly because they have been practically used in diverse fields as adsorbents, catalysts, catalyst supports, low-n and low-k materials, drug delivery carriers, and so on.[1] By general definition, zeolite has its pore diameters in the microporous scale (less than 2 nm), while the pore sizes of mesoporous silica are 2–50 nm. However, silica-based nanoporous materials with pore sizes near the boundary of micro- and mesoporous scales are still rare.[2] This micro–meso transition length scale is of great scientific significance because adsorption behavior can change from monolayer to multi-layer modes, probably making the classical adsorption theories become inapplicable.[3] From a technological viewpoint, moreover, one can expect that different physico-chemical properties can arise from this transition region, thereby providing opportunities for new applications.

Two main approaches can be conceived to achieve silica-based materials having porosity at the micro–meso transition. One is enlarging the micropores of zeolite, while the other is shrinking the pore size of mesoporous silica. The former is exceptionally difficult as such extra-large-pore zeolites tend to be thermodynamically less stable than their counterparts with smaller pores.[4] The pore sizes of

zeolites are generally limited to 1.3 nm,[5] although there are a few exceptions.[2a,b] By the latter approach, a straightforward strategy is to shorten the length of the alkyl or aliphatic chains of structure-directing agents (SDAs), also called surfactants, used to synthesize mesoporous silica, which roughly determines the size of mesopores.[6] It is, however, still challenging to achieve the silica materials with uniform pore sizes at and below 2 nm because the shortened alkyl chains can somewhat lose the self-assembling ability.

Orthogonality, originally termed in mathematics, is defined as the relation of two or more non-overlapping, independent objects or functions. In chemistry, materials science and life science, an orthogonal self-assembly represents hierarchical self-assembling processes that involve multiple interactions, being independent but working together cooperatively in a synergistic way. The orthogonal approach provides a powerful tool to create more complex matters by utilizing the combination of different interactions, being covalent or non-covalent, where modifications can be made to a particular motif without affecting the others.[7] This approach has been widely employed to achieve hierarchical supramolecular assemblies and soft materials. It is also noteworthy that some other supramolecular approaches such as micelle assembly have been successfully applied to synthesize nanoporous architectures with unique properties.[8] We have deemed that the orthogonal assembly may overcome the problems in reducing the pore sizes of mesoporous silica to around 2 nm as the orthogonal interactions of SDA–SDA, SDA–silica, and silica–silica can improve the assembly even for the SDAs with the shortened alkyl chains.

Herein, we report the synthesis of nanoporous silicas having pore apertures near the micro–meso boundary by using novel SDAs that can facilitate multiple, orthogonal interactions (see Fig. 1). To enhance the SDA–SDA interaction, disk-like molecules with rigid, π-conjugated cores have been considered as SDAs because these molecules can interact with each other *via* π–π interactions and thus form one-dimensional stacks. Although ordered columnar assemblies can be formed from molecular disks with, for example, phthalocyanine, triphenylene, and N-donor ligand–metal complex cores,[9] their molecular sizes are too large for the formation of

a Department of Chemical System Engineering, The University of Tokyo, 7-3-1 Hongo, Bunkyo-ku, Tokyo 113-8656, Japan.
E-mail: watcha@chemsys.t.u-tokyo.ac.jp, okubo@chemsys.t.u-tokyo.ac.jp
b Institute of Industrial Science, The University of Tokyo, 4-6-1 Komaba, Meguro-ku, Tokyo, 153-8505, Japan
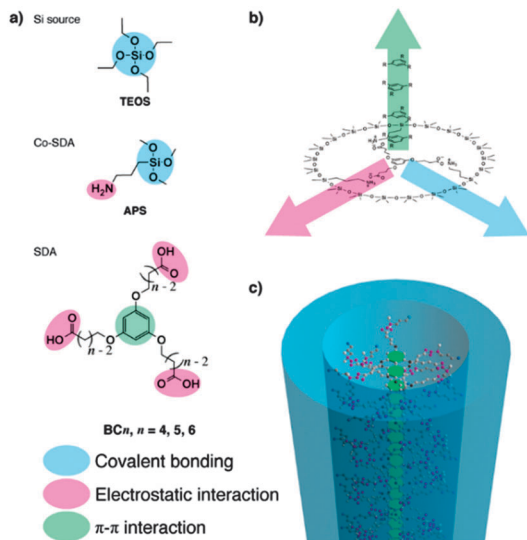
Fig. 1 (a) Molecules and (b) schematic representation of the orthogonal interactions used in this work. (c) Nanoporous silica built through an orthogonal self-assembly approach.

nanopores near the micro–meso boundary. Therefore, a benzene core, the smallest moiety that can form columnar assemblies through π–π stacking,[10] was selected.

The interaction between SDA and silica depends on side chains attaching to the core, namely hydrogen-bonding interaction (for nonionic alkyl polyoxyethylene ether side chains)[9] or electrostatic interaction (for cationic[10] and anionic side chains). Because of its strength, electrostatic interaction is more preferable. Cationic SDAs with a benzene core and long alkyl side chains have been used to synthesize mesoporous silicas.[10] When the cationic alkyl side chains are shortened, however, synthesis of nanoporous silica with smaller, uniform pore sizes is unsuccessful likely because of the weak interactions between positively charged, basic ammonium side chains and negatively charged, weakly acidic silanol (SiOH) groups.[10] Alternatively, we employed here the concept of anionic SDA–co-SDA interaction, established by Yokoi, Che and Tatsumi for the synthesis of anionic surfactant-templated mesoporous silicas (AMSs),[11] in which we have hypothesized that this can critically improve the formation of nanoporous silica because the acidity of anionic SDA ($pK_a \sim 3$–6) is stronger than that of silanol ($pK_a \sim 7$).[11e,12] Based on the aforementioned consideration, novel anionic SDAs (**BCn**, Fig. 1a) were designed and synthesized (see experimental details and characterization in the ESI,† Fig. S1), while **TEOS** (tetraethyl orthosilicate) and **APS** (3-aminopropyltrimethoxysilane) were used as silica source and co-SDA, respectively. The molecular sizes of **BCn** together with **APS** can create the pore sizes near the micro–meso boundary, being 1.5–2.5 nm, as computed by DFT optimization (B3LYP/6-31G(d) level) (see Fig. S2, ESI†). As a co-SDA, **APS** can interact with SDAs via electrostatic interaction and can covalently co-condense with **TEOS** to form silica frameworks.

Learning from natural and biological systems that can use several weak interactions (e.g., π–π stacking, hydrogen-bonding, and electrostatic charge-matching) efficiently in aqueous media at

neutral pH and moderate temperature,[13] nanoporous silicas were synthesized at 60 °C from the starting mixtures with the molar composition of 0.05 **BCn** : x **APS** : $(1 - x)$ **TEOS** : 90 H$_2$O, where x = 0–0.30. The as-made white powder was either calcined at 550 °C for 6 hours or extracted with ammonium acetate in ethanol[11d] (see details in the ESI†). The pH of the starting mixture depends on the amount of **APS** (i.e., an x value), but being close to neutral.

The co-condensation of **APS** and **TEOS** was confirmed by solid-state ^{29}Si magic-angle spinning (MAS) NMR spectroscopy (Fig. S3, ESI†). The signals arising from Q^4, Q^3, Q^2, and T^3 are observed at δ = −111, −101, −91, and −66, respectively (Q^a: $Si(OSi)_a(OH)_{4-a}$; T^b: $CSi(OSi)_b(OH)_{3-b}$), suggesting that both **APS** and **TEOS** co-condense to form silica products. For the sample prepared with **BC6** (x = 0.18), the peak ratio of (Q^2 + Q^3 + Q^4)/T^3, being 4.1, was slightly altered from the initial molar ratio (**TEOS**/**APS** = 4.6) probably because the ethoxy group of **TEOS** is less reactive than the **APS** methoxy group.

Solid-state ^{1}H–^{13}C cross-polarization (CP)/MAS NMR and UV-Vis spectroscopies were used to investigate the presence of organic groups (**APS** and **BCn**) in the as-made products. The as-made silica-**BC6** sample showed the NMR peaks corresponding to the 3-aminopropyl moiety at δ = ca. 10, 22, and 42, in addition to the peaks from **BC6** (Fig. S4, ESI†), confirming that both **APS** and **BCn** are incorporated in the as-made sample. The molar ratios of **BCn**/ **APS** in the as-made sample were almost identical to those of the starting mixtures, as determined by elemental analyses. In UV-Vis spectra (Fig. S5, ESI†), the peaks around 240 nm can be assigned to the π–π stacking of benzene rings of **BCn**.[10,14] Compared to the **BCn** powder, these peaks are blue-shifted when **BCn** was incorporated into the as-made samples, suggesting that the arrangements of **BCn** in the as-made samples are predominant by face-to-face H-aggregation. In the powder form of molecules, **BCn** can arrange in both face-to-face and end-to-end (J-aggregation) modes due to π–π interaction of benzene cores and hydrogen-bonding interaction of carboxylic end-groups, respectively. In the as-made samples, in contrast, **BCn** is likely piled up to form one-dimensional arrangement through π–π interaction, causing the blue-shift in UV-Vis spectra.

Powder X-ray diffraction (XRD) patterns of the products synthesized using SDAs having different lengths of alkyl side chains at varied amounts of **APS** are shown in Fig. 2. The silica products obtained at x = 0.18, in which the molar ratio of COOH/NH$_2$ is close to 1, show broad XRD peaks with a d-spacing of ca. 3 nm, suggesting that they likely possess some periodicity.[15] Among **BCn**, the XRD peaks are more pronounced when the products were synthesized using **BC6**. The products synthesized without **BCn** or **APS** do not show any XRD peaks (see Fig. S6 and S7 in the ESI,† respectively). These results suggest that the presence of both **BCn** and **APS** in the synthesis mixture at the optimal ratio (COOH/NH$_2$ $\sim$ 1) is crucial to promote the electrostatic interaction of SDAs and co-SDA, thereby enhancing the periodicity of the products.

The SEM image (Fig. S8, ESI†) shows that the product has an irregular shape with non-uniform particle size. A typical high-resolution (HR) TEM image of the calcined silica-BC6 sample (x = 0.18) shown in Fig. 3 is translucent, which is indicative of porous characteristics. The pore sizes were estimated to be about 2 nm. As shown in Fig. 3 (inset), the fast Fourier
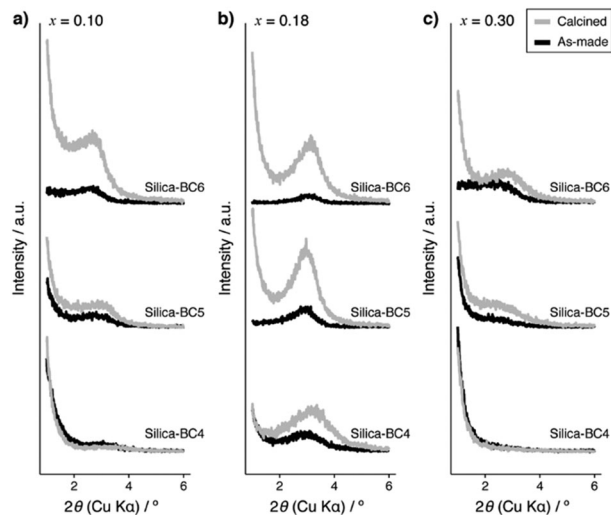
Fig. 2   Powder XRD patterns of the as-made (black line) and calcined (grey line) products synthesized with SDAs having different lengths of alkyl side chains at (a) $x = 0.10$, (b) $x = 0.18$, and (c) $x = 0.30$.

Fig. 4   (a) Nitrogen sorption isotherms (filled and empty symbols representing adsorption and desorption branches, respectively) and (b) the corresponding histograms of NL-DFT pore size distributions of the calcined products synthesized at $x = 0.18$ with SDAs having different lengths of alkyl side chains. In (a), the isotherms of calcined silica-BC5 and calcined silica-BC6 were offset by 300 and 600 cm^3 g^{-1} STP, respectively.

transform (FFT) of the selected area shows a ring pattern, indicating that the selected area possesses some periodicity. Additional HRTEM images are shown in Fig. S9, ESI.†

Nitrogen adsorption–desorption isotherms and their corresponding pore size distributions calculated by a non-local density functional theory (NL-DFT) of the calcined samples are depicted in Fig. 4 ($x = 0.18$) and Fig. S10 ($x = 0.10$ and 0.30; ESI†), together with apparent specific surface areas (calculated by the Brunauer–Emmett–Teller (BET) method), micropore volumes (calculated by the NL-DFT method), and total pore volumes (at $P/P_0 = 0.99$). At $x = 0.18$, the sample prepared with **BC4** shows sharp uptakes at low relative pressure ($P/P_0 < 0.05$) with slightly increasing uptakes at higher relative pressure, indicating that it is a microporous material. In contrast, the samples synthesized with **BC5** and **BC6** show
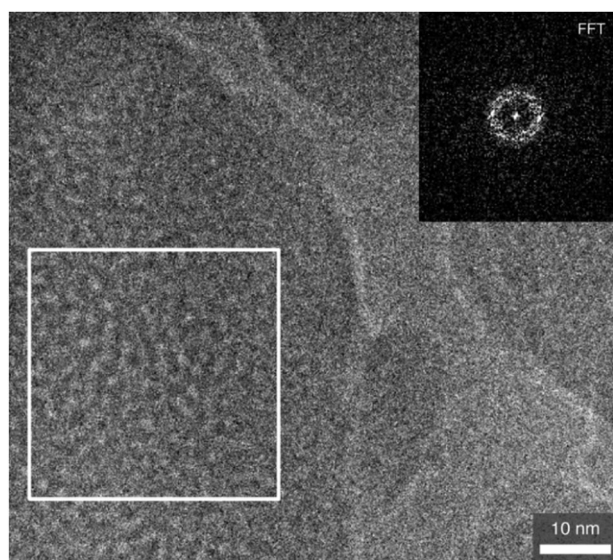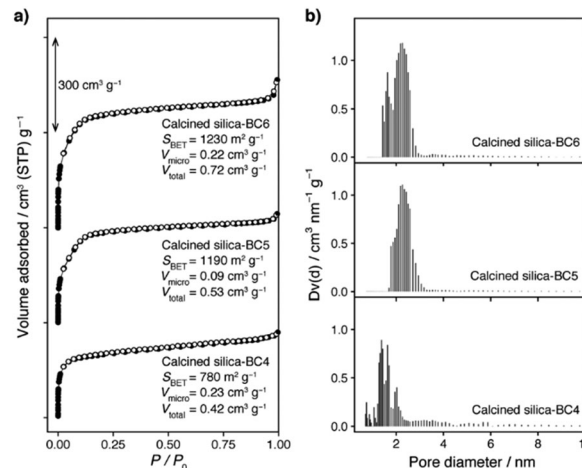

Fig. 3   High-resolution TEM image of the calcined silica-BC6 sample. The inset shows the FFT of the marked area (white frame).

considerably sharp uptakes at P/P_0 up to 0.15, indicating that their nanopores lie on the boundary between micro- and mesoporous regions. Pore diameters were evaluated by the NL-DFT method, being consistent with the molecular sizes of **APS** and **BCn**. The pore size distribution of the sample derived from **BC4** is centered at 1.7 nm, while the samples from **BC5** and **BC6** have pore diameters centered at 2.2 nm. Notably, the pore size distributions become slightly broader with extended carbon chains connected to the benzene core, probably due to the increasing flexibility of the side chains. Similar trends were also observed when $x = 0.10$ and 0.30, with the pore diameters of *ca.* 1.5–3 nm, depending on synthesis conditions and SDAs (Fig. S10, ESI†).

It is now accepted that argon adsorption can give more accurate estimation of the pore size distribution than that calculated from nitrogen adsorption.[16] To confirm the pore size distributions of the resulting materials, argon adsorption was also measured, giving the pore size distributions akin to those obtained from nitrogen adsorption with slightly larger diameters (*ca.* 0.1–0.2 nm) (Fig. S11, ESI†). It should be noted that the estimation of pore size distribution is somewhat sensitive to the pore structure,[16] and therefore further characterization of pore structures (*e.g.*, 1-dimensional cylindrical or 3-dimensional interconnected pores) should be conducted in the future.

The apparent specific BET surface area, micropore volume, and total pore volume are increased as the length of side carbon chains increased (see Fig. 4 and Fig. S10, ESI†). The highest values are observed for the silica synthesized at $x = 0.18$ with **BC6**, being 1230 m^2 g^{-1} (surface area), 0.22 cm^3 g^{-1} (micropore volume), and 0.72 cm^3 g^{-1} (total pore volume). To the best of our knowledge, these results are the highest values reported for AMSs.[11] It is noteworthy that the products obtained without the addition of **APS** are mesoporous silica with lower BET surface areas and very broader pore size distributions (Fig. S7, ESI†) whereas the product synthesized without **BCn** shows very low

BET surface area (Fig. S6, ESI†), again indicating that the presence of both **BC*n*** and **APS** is a vital requirement to achieve highly nanoporous silicas with pore apertures near the boundary between micro- and mesopores (*vide supra*).

Due to the non-covalent bonding of **BC*n*** and **APS**, removal of **BC*n*** by extraction was also investigated to potentially produce nanoporous silica with amine functional groups,[11] demonstrated here for the silica synthesized at $x = 0.18$ with **BC6**. After three times of extraction, the removal of **BC6** was evidenced by ^1H–^{13}C CP/MAS NMR and UV-Vis spectroscopies (Fig. S4 and S5, respectively, ESI†). As shown in Fig. S4 (ESI†), only resonance signals corresponding to **APS** are observed, suggesting that **BC6** can be removed, while the **APS** moiety is still intact with the silica frameworks. This was further confirmed by ^{29}Si MAS NMR, showing that the $(Q^2 + Q^3 + Q^4)/T^3$ peak ratio of the extracted sample is similar to that of the as-made one (Fig. S3, ESI†). It should be noted that in comparison with the as-made sample the peak area of Q^3 silicon with respect to Q^4 was slightly decreased upon both extraction and calcination, suggesting that some parts of silanol groups on/in the silica wall are condensed to form new Q^4 silicon. The extracted sample exhibited a BET surface area of 730 $m^2\ g^{-1}$, a micropore volume of 0.06 $cm^3\ g^{-1}$, and a total pore volume of 0.35 $cm^3\ g^{-1}$ (Fig. S12, ESI†). The reduction in porosity is partly due to the incomplete extraction of **BC6** (about 20% remain), as suggested by the CHN elemental analyses (Table S1, ESI†). Further improvement of extraction conditions should be studied in the future. Note that the nitrogen content in the extracted sample is about 2 mmol g^{-1}. The presence of such amine groups in the extracted samples can be useful for several applications, for example, in base catalysis, CO_2 adsorption, and drug delivery.[1]

In summary, nanoporous silicas having some periodicity, high surface area, and pore diameters near the micro–meso transition region are synthesized using novel SDAs with aromatic cores and anionic end-groups. Their BET surface areas are among the highest values reported for nanoporous silicas. The pore diameters can be altered across the boundary between micro- and mesopores, ranging from 1.5 to 3 nm, depending on the size of SDAs (**BC*n***) and the amount of co-SDA (**APS**). A possible formation scheme can be explained based on multiple, orthogonal interactions between SDAs, co-SDAs and silica frameworks. Upon dissolution in water, co-SDAs are deprotonated and they electrostatically interact with SDAs. Meanwhile, SDAs interact with each other *via* π–π interactions. Finally, the co-SDA and silica source co-condense to form the silica frameworks. We believe that although more studies are needed to understand the structure-directing mechanisms, this orthogonal approach can be extended to synthesize nanoporous silica with more complex functionality, which merits future investigation.

Notes and references

1 (*a*) M. E. Davis, *Nature*, 2002, **417**, 813; (*b*) K. Ariga, A. Vinu, Y. Yamauchi, Q. Ji and J. P. Hill, *Bull. Chem. Soc. Jpn.*, 2012, **85**, 1; (*c*) K. Kuroda, A. Shimojima, K. Kawahara, R. Wakabayashi, Y. Tamura, Y. Asakura and M. Kitahara, *Chem. Mater.*, 2014, **26**, 211; (*d*) Y. Yamauchi, *J. Ceram. Soc. Jpn.*, 2013, **121**, 831; (*e*) N. L. Torad, M. Naito, J. Tatami, A. Endo, S.-Y. Leo, S. Ishihara, K. C.-W. Wu, T. Wakihara and Y. Yamauchi, *Chem. – Asian J.*, 2014, **9**, 759.
2 (*a*) J. Jiang, J. L. Jorda, J. Yu, L. A. Baumes, E. Mugnaioli, M. J. Diaz-Cabanas, U. Kolb and A. Corma, *Science*, 2011, **333**, 1131; (*b*) J. Sun, C. Bonneau, Á. Cantín, A. Corma, M. J. Díaz-Cabañas, M. Moliner, D. Zhang, M. Li and X. Zou, *Nature*, 2009, **458**, 1154; (*c*) L. Zhang, Q. Yang, H. Yang, J. Liu, H. Xin, B. Mezari, P. C. M. M. Magusin, H. C. L. Abbenhuis, R. A. van Santen and C. Li, *J. Mater. Chem.*, 2008, **18**, 450.
3 (*a*) R. F. Lobo, *Nature*, 2006, **443**, 757; (*b*) J. Rouquerol, F. Rouquerol, K. S. W. Sing, P. Llewellyn and G. Maurin, *Adsorption by Powders and Porous Solids: Principles, Methodology and Applications*, Academic Press, Oxford, 2nd edn, 2014.
4 J. Jiang, J. Yu and A. Corma, *Angew. Chem., Int. Ed.*, 2010, **49**, 3120.
5 (*a*) A. Corma, M. J. Díaz-Cabañas, J. L. Jordá, C. Martínez and M. Moliner, *Nature*, 2006, **443**, 842; (*b*) J. Jiang, J. L. Jorda, M. J. Diaz-Cabanas, J. Yu and A. Corma, *Angew. Chem., Int. Ed.*, 2010, **49**, 4986.
6 J. S. Beck, J. C. Vartuli, W. J. Roth, M. E. Leonowicz, C. T. Kresge, K. D. Schmitt, C. T-W. Chu, D. H. Olson, E. W. Sheppard, S. B. McCullen, J. B. Higgins and J. L. Schlenker, *J. Am. Chem. Soc.*, 1992, **114**, 10834.
7 (*a*) S.-L. Li, T. Xiao, C. Lin and L. Wang, *Chem. Soc. Rev.*, 2012, **41**, 5950; (*b*) E. Elacqua, D. S. Lye and M. Weck, *Acc. Chem. Res.*, 2014, **47**, 2405; (*c*) R. K. Iha, K. L. Wooley, A. M. Nyström, D. J. Burke, M. J. Kade and C. J. Hawker, *Chem. Rev.*, 2009, **109**, 5620; (*d*) E. M. Sletten and C. R. Bertozzi, *Angew. Chem., Int. Ed.*, 2009, **48**, 6974.
8 (*a*) C. Li, Ö. Dag, T. D. Dao, T. Nagao, Y. Sakamoto, T. Kimura, O. Terasaki and Y. Yamauchi, *Nat. Commun.*, 2015, **6**, 6608; (*b*) H. Wang, S. Ishihara, K. Ariga and Y. Yamauchi, *J. Am. Chem. Soc.*, 2012, **134**, 10819.
9 (*a*) M. Kimura, K. Wada, K. Ohta, K. Hanabusa, H. Shirai and N. Kobayashi, *J. Am. Chem. Soc.*, 2001, **123**, 2438; (*b*) A. Okabe, T. Fukushima, K. Ariga and T. Aida, *Angew. Chem., Int. Ed.*, 2002, **41**, 3414; (*c*) H. O. Lintang, K. Kinbara, K. Tanaka, T. Yamashita and T. Aida, *Angew. Chem., Int. Ed.*, 2010, **49**, 4241.
10 Y. Fukasawa, A. Sugawara, H. Hirahara, A. Shimojima and T. Okubo, *Chem. Lett.*, 2010, **39**, 236.
11 (*a*) T. Yokoi, H. Yoshitake and T. Tatsumi, *Chem. Mater.*, 2003, **15**, 4536; (*b*) S. Che, A. E. Garcia-Bennett, T. Yokoi, K. Sakamoto, H. Kunieda, O. Terasaki and T. Tatsumi, *Nat. Mater.*, 2003, **2**, 801; (*c*) T. Yokoi, H. Yoshitake, T. Yamada, Y. Kubota and T. Tatsumi, *J. Mater. Chem.*, 2006, **16**, 1125; (*d*) H. Zheng, C. Gao and S. Che, *Microporous Mesoporous Mater.*, 2008, **116**, 299; (*e*) L. Han and S. Che, *Chem. Soc. Rev.*, 2013, **42**, 3740.
12 (*a*) N. A. Brunelli, K. Venkatasubbaiah and C. W. Jones, *Chem. Mater.*, 2012, **24**, 2433; (*b*) N. A. Brunelli and C. W. Jones, *J. Catal.*, 2013, **308**, 60.
13 (*a*) D. Philp and J. F. Stoddart, *Angew. Chem., Int. Ed. Engl.*, 1996, **35**, 1154; (*b*) L. M. Greig and D. Philp, *Chem. Soc. Rev.*, 2001, **30**, 287; (*c*) A. Corma, M. J. Díaz-Cabañas, M. Moliner and G. Rodríguez, *Chem. Commun.*, 2006, 3137.
14 (*a*) D. Xu, Y. Ma, Z. Jing, L. Han, B. Singh, J. Feng, X. Shen, F. Cao, P. Oleynikov, H. Sun, O. Terasaki and S. Che, *Nat. Commun.*, 2014, **5**, 4262; (*b*) B. K. Singh, D. Xu, L. Han, J. Ding, Y. Wang and S. Che, *Chem. Mater.*, 2014, **26**, 7183.
15 W. Chaikittisilp, A. Sugawara, A. Shimojima and T. Okubo, *Chem. Mater.*, 2010, **22**, 4841.
16 M. Thommes and K. A. Cychosz, *Adsorption*, 2014, **20**, 233.